# Helios Spin Modulation Simulation Tests

N. C. Ham
R.F. Systems Development Section

*Additional analysis and study have completed the mathematical model of the Helios spacecraft low-gain antenna and permitted the formulation of experimental tests for simulating the spin modulation effects at a typical Deep Space Station communication system. The details of the test technique, system test configuration, and results of the simulation tests are explained.*

## I. Introduction

Previous analysis and study of the Helios low-gain antenna (LGA) were covered by Ref. 1, in which a mathematical model of the LGA was developed, with particular emphasis on the region of signal interferometry.

As a result of this modeling effort, a better understanding of the affected telecommunication link elements was achieved thus permitting formulation of realistic experimental tests by simulating these effects at a typical Deep Space Station communication system.

This article is a study extension of the LGA mathematical model, detailing the experimental test technique and results of the simulation testing that was performed at the JPL Compatibility Test Area, (CTA 21).

## II. LGA Mathematical Model

The general equation of the mathematical model used in Ref. 1 follows:

$$E_S\,\gamma = E_D\left[1 + \left(\frac{E_H}{E_D}\right)^2 + 2\left(\frac{E_H}{E_D}\right)\cos\beta\right]^{1/2} \times \sqrt{\arctan\left(\frac{\frac{E_H}{E_D}\sin\beta}{1 + \frac{E_H}{E_D}\cos\beta}\right)} \qquad (1)$$

where $E_S\,\gamma$ is the magnitude and phase of the resultant combined signal of the dipole and horn radiated signals

($E_D$ and $E_H$, respectively) of similar polarization, and $\beta$ is the relative phase angle between the radiated signals.

Figure 1 is a reproduction of the computer plot and measured data comparison (from Ref. 1) of the carrier signal phase variation vs the spacecraft rotational angle for one complete rotation. A study of the figure reveals poor correlation near the region of $\phi = 180$ deg due to the assumed initial lead phase angle relationship between the horn and dipole antenna signals.

Figure 2 illustrates the spacecraft mockup test setup used to measure the resultant LGA radiation patterns. The reference antenna shown is used as the reference signal input to the network analyzer, while the LGA provides the input to the other terminal, which is designated the measured input. The phase relation of the reference antenna signal to the LGA signal, both of which are received from the radiating test antenna, is an initial phase condition that must be accounted for in the mathematical model. This initial condition is different for each value of the aspect angle (the angle formed by the spacecraft Z-axis and the centerline of the test antenna); this angle is set for a pattern test prior to rotating the spacecraft about the Z-axis. Associated with this phase relation between the reference signal and the LGA signal is an internal phase relation, within the spacecraft microwave circuitry, between the horn and dipole antenna.

Figure 3 depicts these initial phase conditions for a specific aspect angle. Figure 3a is the vector diagram, where only the internal phase is considered, and Fig. 3b shows the relation with the phase of the test measurement physical configuration included; $\beta$ is the horn antenna internal leading phase angle, and $\Omega$ is the initial phase existing between the reference and LGA antenna signals. Also shown are the expressions for the resultant phase angle (combined horn and dipole signals) due to these conditions.

The computer plot of the configuration expression of Fig. 3b,

$$\gamma = \Omega + \arctan\left(\frac{1 + \frac{E_H}{E_D}\sin\beta}{\frac{E_H}{E_D}\cos\beta}\right) \qquad (2)$$

is shown in Fig. 4, where $\Omega$ is set to a value of 90 deg.

Figure 5 is a recomparison of the new computer plot to the measured antenna pattern previously shown, and reveals a better correlation at $\phi = 180$ deg.

Suffice it to say, the mathematical model, to a first approximation, is a valid representation of the Helios LGA. The goal for its development was to assess the nature of the rapid phase deviation of the carrier signal in the interferometry region in terms of its discontinuity (i.e., varying $\pm\infty$ deg) or its deviation in known and predictable magnitudes.

The assumption, derived from the model and measured patterns, is that the periodicity of the amplitude and phase variations is an average 25 Hz per spacecraft revolution (at 1 revolution per second). Similarly, the respective magnitude of these variations can be tabulated from the measured patterns made wih various aspect angles and combinations of polarized signals, namely, right circular polarization (RCP), and horizontal or vertical linear polarization.

## III. Spin-Modulation Variable Values

A summary of the spin-modulation effects is shown in Fig. 6 for the downlink signal case, where the ground receiving system is polarized for RCP.

The amplitude modulation variation shown, as a function of the aspect angle, is the magnitude of the significant average values that occur per spacecraft revolution at the specific aspect angle. The average is a visual integration of the measured pattern response whereby the deep nulls with narrow width are integrated and normalized; the normalizing value is determined by the pulse duration of the 128 and 256 symbol-per-second pulse-code modulation (PCM) telemetry data and the receiver automatic gain control (AGC) loop bandwidth.

The rationale for determining the average value follows: to simulate the actual varying magnitude response pattern per spacecraft revolution requires a complex function generator or computer program that would be costly. Instead, the use of a constant-magnitude continuous-simulation waveform equal to the average value simplifies the testing and should be a valid representation of the effect.

The magnitude of the phase modulation within the interferometry region is similarly obtained from the measured patterns. The heavy lines indicate the predomi-

nant magnitude per spacecraft rotation over the interferometry span of the aspect angle. In other words, the large phase modulation (PM) variations (>90 deg) occur for only a small percentage of one revolution. For aspect angles greater than 50 deg, the phase variation magnitude is fairly constant per revolution, decreasing in value as the aspect angle increases.

The frequency modulation (FM) effect was not covered by the mathematical model and was only briefly treated in Ref. 2; therefore, it will be further expanded here.

The FM effect is caused by the horn element of the LGA because of the horn's physical offset of approximately 6.5 $\lambda$ (wavelength at the downlink frequency) from the spin axis, and takes the form of an added doppler frequency component, $\Delta F_D = \sin \psi\ 6.5\lambda \sin 2\Pi f_s t$, varying about the normal Earth radial velocity doppler frequency (Fig. 7). Here $f_s$ is the spacecraft rotational rate and $\psi$ is the aspect angle. For the stabilized condition of 1 revolution per second, the equation becomes $\Delta F_D = \sin \psi\ 13\Pi \sin 2\Pi t$, where $13\Pi = 6.5\ \lambda$ because $2\Pi$ radians occur for one wavelength. Thus, for the RCP mode, the FM deviation increases as a function of the aspect angle to a maximum value of approximately 28 Hz at an aspect angle of 40 deg, and rapidly decreases at greater angles because the gain of the RCP horn is decreasing and the gain of the dipole antenna is increasing.

Since the FM occurs at a 1-Hz rate, the maximum rate of change of frequency deviation, or doppler rate, occurs at the aspect angle producing the maximum frequency. For example, the 28-Hz magnitude is equivalent to an effective offset displacement of 4.2 $\lambda$, (i.e., 6.5 $\lambda$ × sin 40 deg); by differentiation of the deviation expression,

$$\begin{aligned} \Delta \dot{F}_D &= \frac{d}{dt}(8.4\Pi \sin 2\Pi t) \\ &= -16.8\Pi^2 \cos 2\Pi t \end{aligned} \tag{3}$$

or $\Delta \dot{F}_D = -165 \cos 2\Pi t$ Hz/s. It is this rate of change of doppler that has a stressing effect on the receiver carrier phase-locked loop.

Figure 8 is the similar characteristic where the ground receiving antenna can be configured to receive either horizontal linear or vertical linear polarization. When the horizontal linear mode (for aspect angles from 0 to 50 deg) that is orthogonal to the vertically polarized spacecraft dipole LGA is used, the interferometry amplitude modulation (AM) effects are less severe than those in the RCP reception case; however, the FM effect is greater, since the rotating horn antenna now remains dominant over a greater range of aspect angles. The result is that $\Delta F_D$ and $\dot{F}_D$ reach maximum values of 31 and 197 Hz/s, respectively, at the aspect angle of 50 deg. Associated with the FM deviation are some low PM deviations of ±15 deg near this region.

During the vertical linear reception mode, the vertical linear component of the RCP horn element and the normal vertical linear signal from the dipole element combine to create interferometry effects (as in the RCP case) within the range of aspect angles of 40 to 50 deg.

## IV. Simulation Test Model

Figure 9 is a functional block diagram depicting the simulation model that is used for obtaining experimental test data resulting from spin modulation effects.

The spin modulation effects FM, PM, and AM are separated to permit stimulating the transmission system, at various magnitudes and rates, either individually or combined, in concert with the values determined and delineated in the preceding section. Similarly, the data signal can be adjusted separately to phase-modulate the system; this is the primary modulation for evaluating spin modulation effects.

The FM signal is $e_{FM}(t) = E_1 \sin 2\Pi t$, where the magnitude $E_1$ sets the peak frequency deviation, $\pm F_D$, and $2\Pi t$ is the 1-Hz rotational rate of the spacecraft.

The PM signal

$$e_{PM}(t) = \frac{2}{\Pi} E_2 \left(\sin 2\Pi 25t - \frac{1}{2}\sin 4\Pi 25t + \frac{1}{3}\sin 6\Pi 25t - \cdots\right)$$

represents the Fourier series for a sawtooth waveform and is illustrated in Fig. 10 for the fundamental frequency of 25 Hz.

Similarly, the AM signal

$$e_{AM}(t) = \frac{2}{\Pi} E_3\left(1 + \frac{2}{3}\cos 4\Pi 12.5t - \frac{2}{15}\cos 8\Pi 12.5t - \frac{2}{35}\cos 12\Pi 12.5t + \cdots\right)$$

is the Fourier series of a full-wave rectified sine wave, which is used to simulate the interferometry amplitude variation characteristics. Figure 11 illustrates this waveform, where the fundamental sine-wave frequency is set to 12.5 Hz to drive the bridge rectifier, whose output is the desired signal with a periodicity of 25 Hz.

The data signal is comprised of a square-waveform subcarrier, at a fundamental frequency of approximately 32 kHz, biphase-modulated by the information data symbol expressed as $e_D(t) = E_{sc}\,\mathrm{Sin}(\omega_c t + m_p\,\mathrm{Cos}\,\omega_{sy}t)$, where $E_{sc}\,\mathrm{Sin}\,\omega_{sc}t$ is the subcarrier square-waveform, $m_p$ is the biphase-modulation index ($\pm$90 deg), and $\mathrm{Cos}\,\omega_{sy}t$ is the square-waveform pseudo-noise (PN) sequence. The data symbol rate is set to values of 128 symbols per second (SPS) to simulate the uncoded telemetry mode, or to 256 SPS to simulate the convolutionally-coded rate half-mode.

The space attenuation simulation is achieved by the variable attenuator and determines the values of the carrier power, $P_c$, and sideband power S. The ratio of $P_c$ to S is set by the data signal amplitude $E_{sc}$ — the modulation index. The exact value of the space attenuation is determined by the desired value of the carrier power to noise spectral density ratio $P_c/N_0$, or data power per symbol rate to noise spectral ratio $ST_s/N_0$.

In the case of obtaining simulation data with no applied data modulation, the characteristics of the carrier phase-locked loop (PLL) are evaluated and the $P_c/N_0$ ratio is normalized to an independent variable $M$, which is the margin in decibels above the loop threshold signal level, and carrier cycle slippage to the dependent variable.

When data modulation is applied, $ST_s/N_0$ is the independent variable, and symbol error rate the dependent variable.

## V. System Test Configuration

Figure 12 is the functional block diagram of the system test configuration used at CTA 21.

The method of setting the magnitude of the frequency deviation (or FM) was first to determine the sensitivity value of the exciter voltage-controlled oscillator (VCO) (which was 400 Hz/peak volts) and then to adjust the output level of the 1-Hz sine-wave generator to 10,000 times the desired frequency deviation, followed by inserting a 40-dB attenuator in series with the generator/VCO interface. For example, the $\Delta F_D$ desired was $\pm$31 Hz at S-band; thus, the peak voltage setting is $E_1$ = (31 Hz $\times$ 10,000)/(96 $\times$ 400 Hz/V) = 0.08 V peak, where 96 is the frequency multiplication factor of the exciter.

An "L" network, consisting of a series element of 100,000 Ω and a 50-Ω shunt element, was used to terminate the 50-Ω, 40-dB attenuator and high input impedance of the VCO input terminal.

The information data simulating the downlink telemetry were obtained from the Simulation Conversion Assembly (SCA), which provided the square-wave subcarrier biphase-modulated by the square-wave PCM data. The PCM data were also simultaneously sent to the Symbol Synchronizer Assembly (SSA) as reference symbols for comparison against the detected data to compute symbol error rate (SER) statistics.

The carrier modulation index, when modulated by the information data, is established by the carrier suppression method, where the suppression $P_c/P_T$ = 20 log cos (phase deviation angle). This suppression was measured by the offset oscillator-mixer and wave-analyzer assemblies.

In like manner, the PM 25-Hz sawtooth waveform was used to phase-modulate the exciter carrier, and the magnitude of the sawtooth peak-to-peak waveform $E_2$ was set by using the calibration values of the exciter phase modulator obtained from the data/subcarrier signal $E_{sc}$.

The AM function generator, as shown in Fig. 11, was connected to PIN modulator circuitry to amplitude-modulate the S-band signal by absorption modulation. The degree of AM was set by monitoring the carrier signal, which was translated by the offset-oscillator mixer to 20 kHz, until the desired modulation depth was achieved as observed on the modulation envelope display on an oscilloscope.

The variable attenuator is used to establish the receiver input to the desired level, which is measured by the Y-factor measuring assembly. The values of $ST_s/N_0$ and $P_c/N_0$ are the variables changed during the simulation tests.

The carrier loop cycle slip information was recorded by connecting the output of the doppler extractor (0 and 90-deg output ports) to a strip chart recorder. Since the extractor provides the doppler at ¼ the S-band value, each cycle slip of the carrier PLL appears as a 90-deg (or

¼-cycle) change, which is easily discernible as a permanent record on the strip chart recorder. Hence, for a given signal level setting, the strip chart recorder is started and time marks are made on the chart 10 min apart for subsequent data reduction.

## VI. Test Sequence and Results

The first experimental test run was conducted by formulating the worst-case conditions when the RCP mode is used for receiving the downlink signal. A review of Fig. 6 reveals that this condition occurs at the aspect angle of 45 deg where the AM is 15 dB peak-to-peak (p–p) and the PM is ±150 deg p–p. Secondary condition values of 15 dB p–p AM and ±90-deg PM (for the aspect angle of approximately 52 deg) and similar values in conjunction with ±30-Hz FM (for the aspect angle of 40 deg) were also selected.

The sequence for obtaining test data is as follows: (1) The values for a particular test condition AM, PM, or FM spin modulation were adjusted as previously discussed; (2) the data rate and modulation index (MI) were selected and set; (3) the receiving/telemetry system loop bandwidth values were set; (4) the RF signal level, or $ST_s/N_0$, was set or measured by the Y-factor technique (performed with data and spin modulation off); (5) the data and appropriate spin modulation were applied; (6) the test was run for an appropriate length of time to gather SER statistics at the Telemetry and Command Processor (TCP) output. The sequence was then repeated at different settings of signal level.

Figure 13 shows the results when the values of AM and PM shown were utilized as the spin modulation parameters. The receiver RF PLL was set to 152 Hz, the AGC loop bandwidth (BW) to wide, the Subcarrier Demodulator Assembly (SDA) and SSA BWs to medium, and the information data at 256 bits/s (uncoded) to produce a carrier modulation index of 42 deg. Also shown are the results when ±30-Hz FM together with 15-dB AM, and ±38-Hz FM with 15-dB AM were applied in conjunction with the information data. The performance characteristics of the ideal coherent phase-shift-keyed (PSK) curve are also shown as a reference to indicate the degree of degradation resulting from spin-modulation effects.

Figure 14 shows the test results where the spin modulation values were ±90-deg PM plus 15-dB AM, with the information data rate at 256 SPS and the receiver PLL bandwidth, as the parameter, set to 48- and 152-Hz values.

A recheck of Fig. 8 for the linear polarized reception mode shows that the AM and PM values are less severe than in the RCP mode. However, the FM deviation increases as the aspect angle increases, particularly for the horizontal linear polarization mode. This is due to the orthogonal rejection of the vertical linear polarized signal from the dipole antenna and permits the horn to remain dominant for greater values of aspect angles. Figure 15 shows the results of the spin modulation effects for this horizontal linear condition where the AM values were 7.5 to 9 dB, PM was constant at ±15 deg, and the FM deviation frequencies were 31 and 36 Hz. These parameters are shown grouped in the respective combinations, where the additional parameters used were the symbol rates at 256 and 128 SPS and the exciter modulation index was set to 42 and 55 deg.

To gain insight into the individual contribution to the system degradation from the spin modulation effects, Fig. 16 shows the results of the tests when ±90-deg PM only, and 15-dB AM spin modulation only, were applied.

Similarly, the RF carrier PLL cycle slippage characteristics show the sensitivity of this loop to the spin modulation effects, and Fig. 17 illustrates the results for the loop bandwidth of 152 Hz. As one would expect, the ±150-deg PM requires a greater margin level than the ±90-deg PM value for a given number of cycles slipped, and the addition of the AM component has a devastating effect.

Figure 18 illustrates a similar test result and test condition, with the PLL bandwidth set to 48 Hz, and shows that a greater margin level above the spin-modulation reference condition is required for the same cycle slippage rate than in the case of the wider loop bandwidth value. This is as expected, since the wider bandwidth loop, as it becomes wider at larger margin levels, tends to track out more of the PM sawtooth sideband frequency components (see Fig. 19).

# References


1. Ham, N. C., "Helios Spacecraft Low-Gain Antenna Model," in *The Deep Space Network Progress Report*, Technical Report 32-1526, Vol. XVIII, pp. 147–162. Jet Propulsion Laboratory, Pasadena, Calif., Dec. 15, 1973.

2. Ham, N. C., "Amplitude and Frequency Modulation Effects to Telemetry Link Reception," in *The Deep Space Network Progress Report*, Technical Report 32-1526, Vol. XIV, pp. 149–160. Jet Propulsion Laboratory, Pasadena, Calif., Apr. 15, 1973.

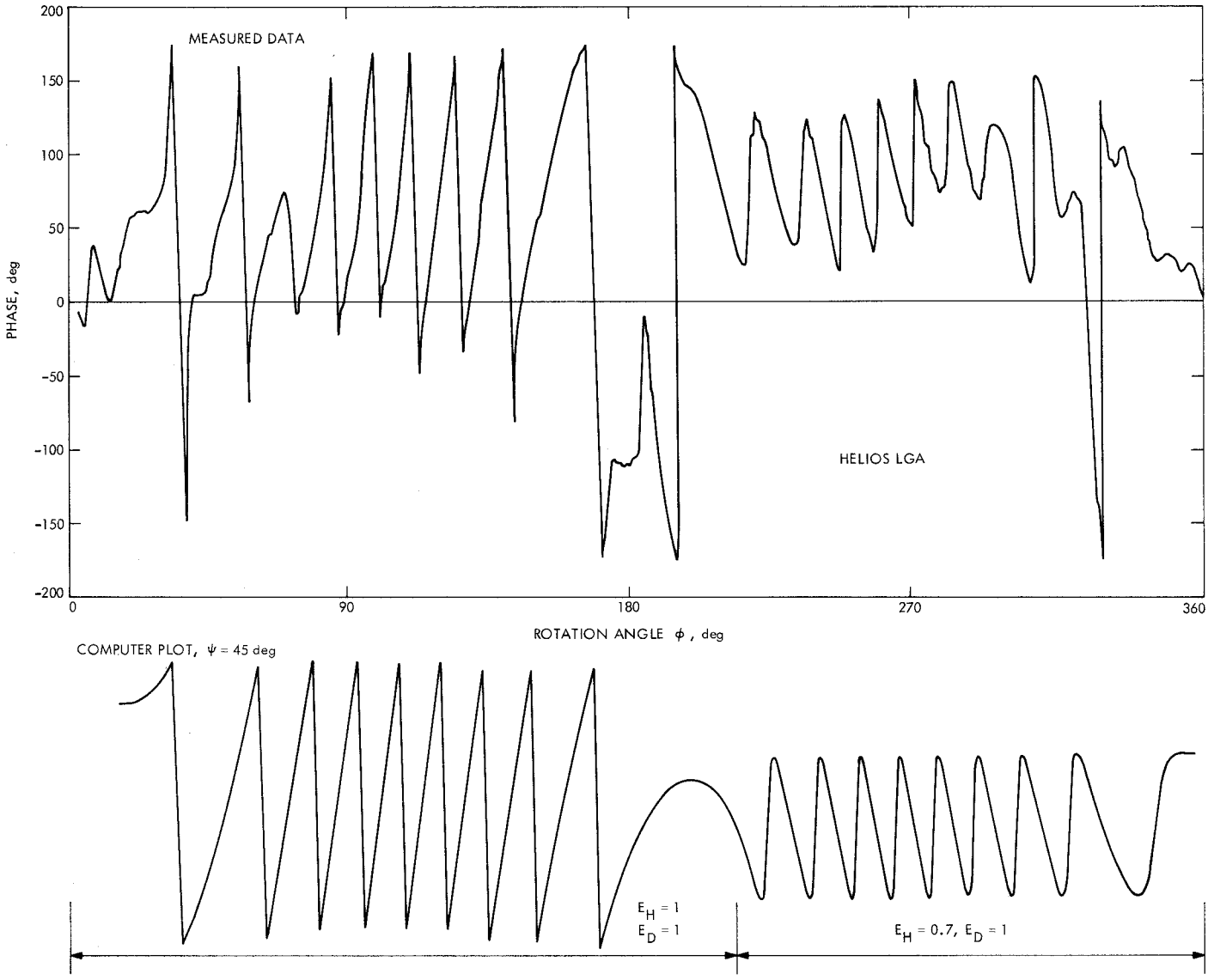


**Fig. 1. Computer plot vs measured phase data, $\psi = 46$ deg**

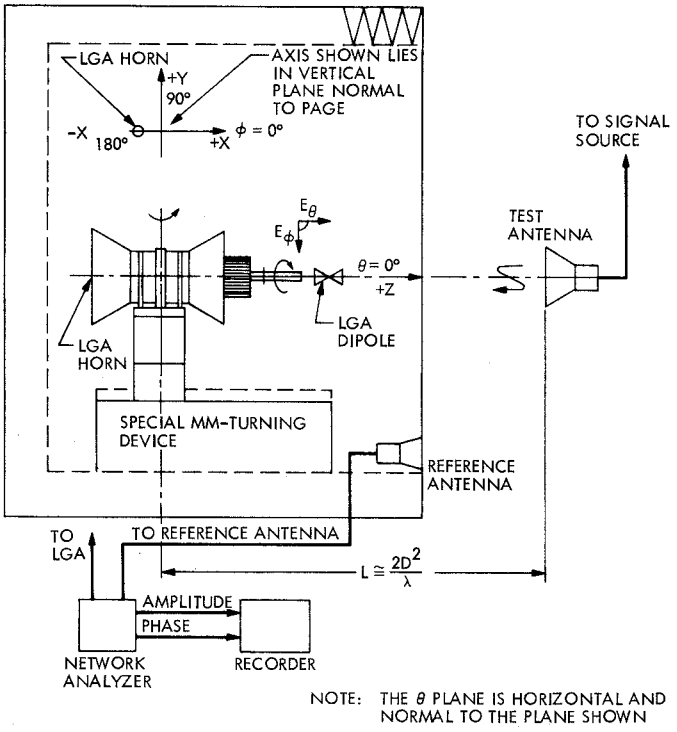


**Fig. 2. Radiation pattern test setup**

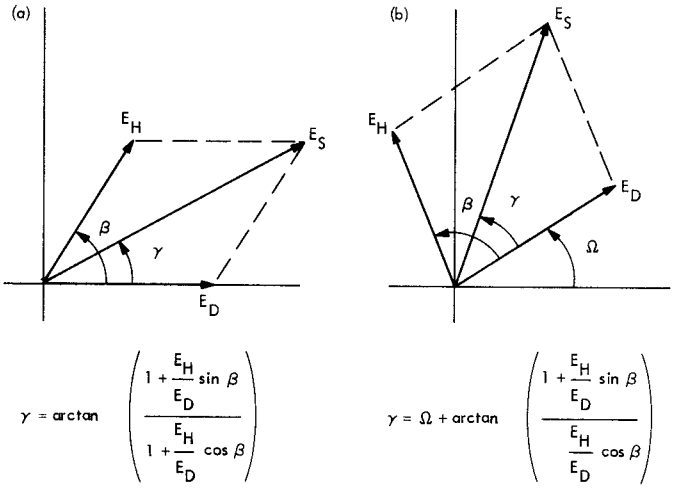


**Fig. 3. Initial LGA phase relations: (a) within spacecraft at $\phi$ = 0 deg; (b) within spacecraft plus measurement configuration at $\phi$ = 0 deg**

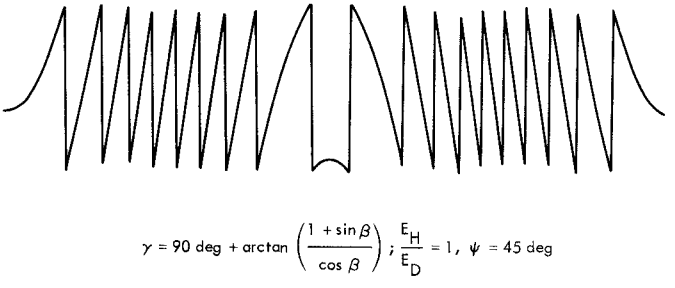


**Fig. 4. Computer plot with initial phase conditions of Fig. 3b**

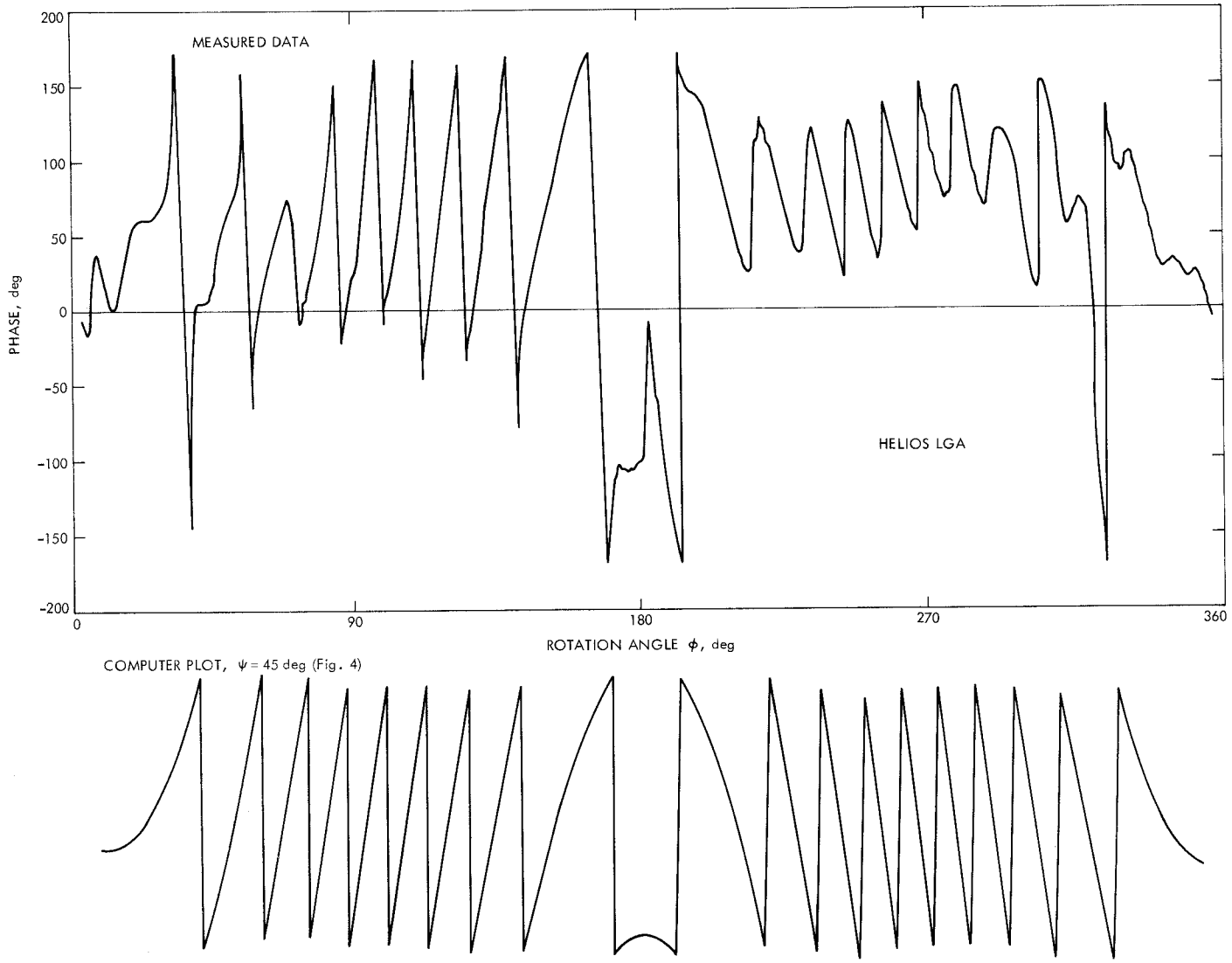


**Fig. 5. Comparison with new computer plot**

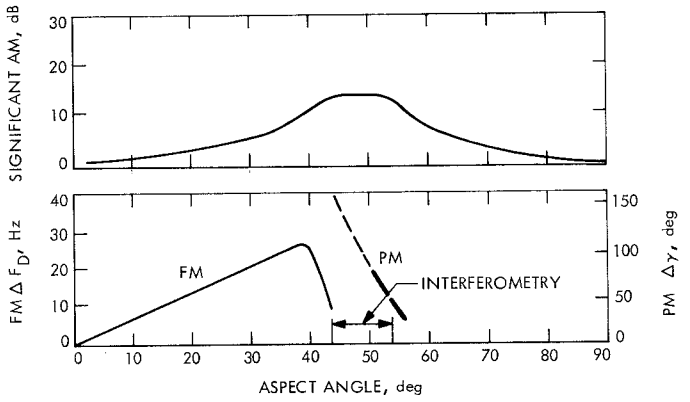


**Fig. 6. Summary of spin modulation effects vs aspect angle for RCP**

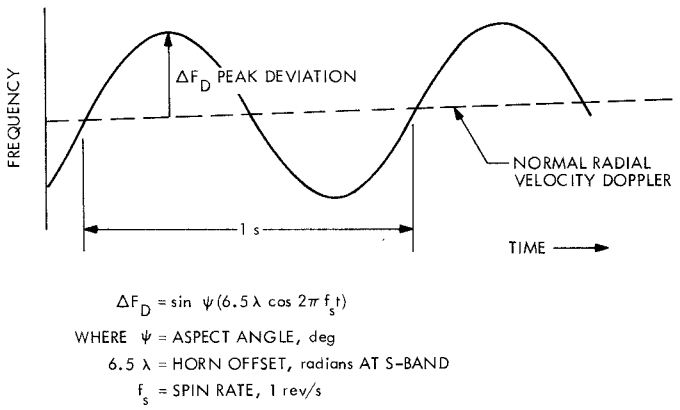


**Fig. 7. Instantaneous doppler variation**

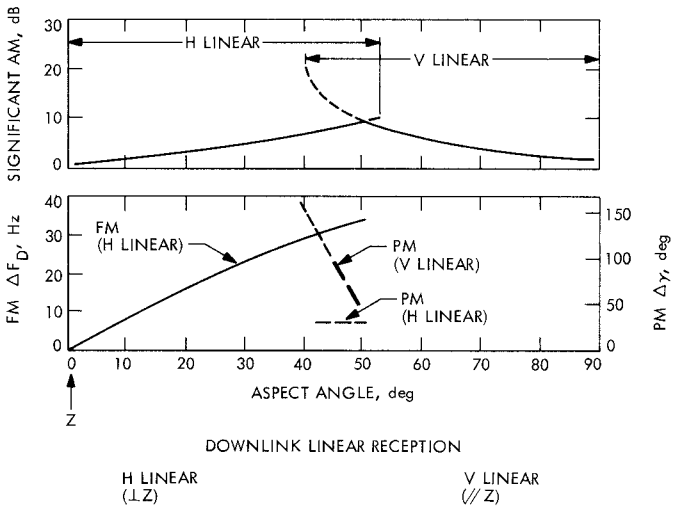


**Fig. 8. Summary of spin modulation effects vs aspect angle for linear polarization**

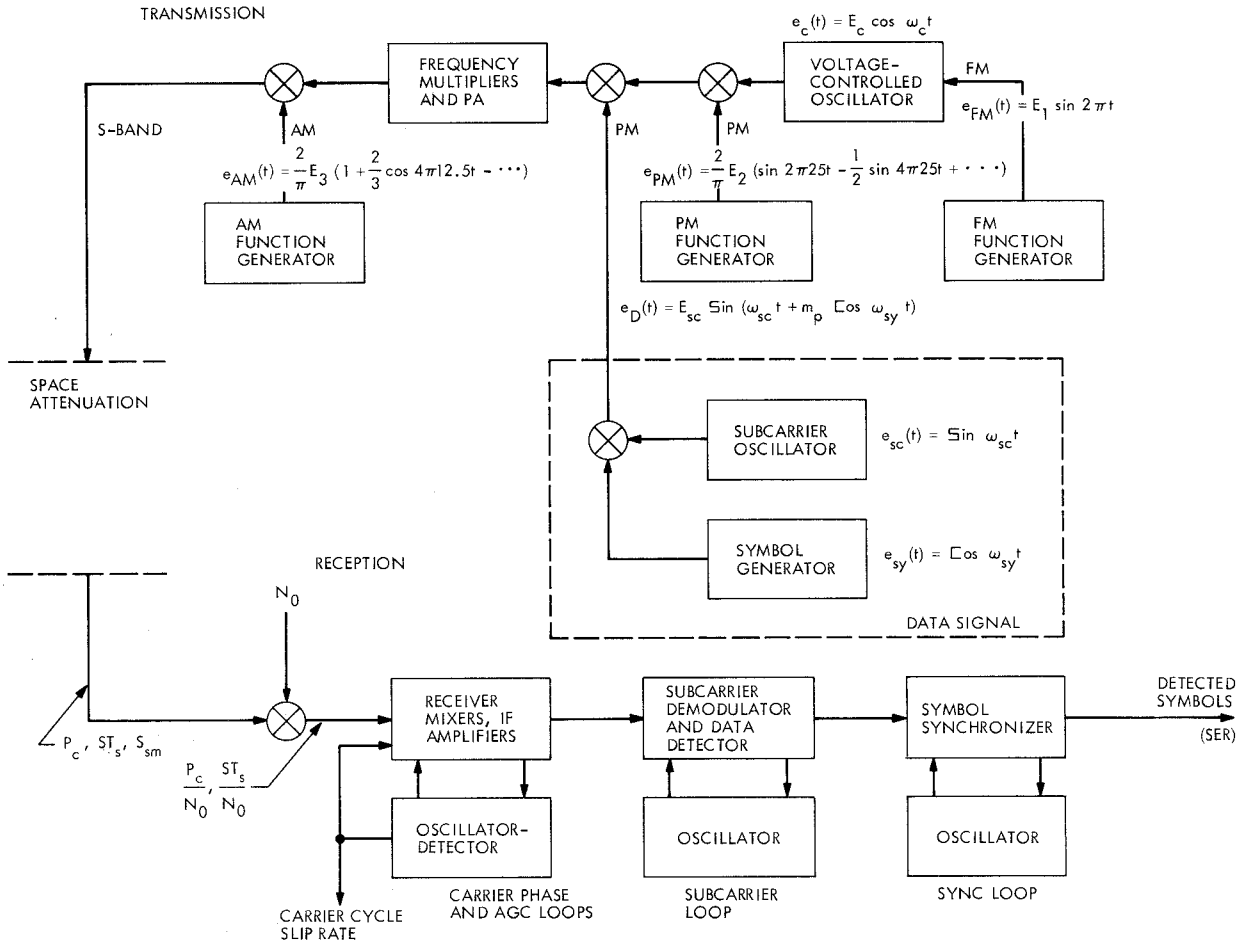


**Fig. 9. Spin modulation simulation model**

FOURIER SERIES FOR PHASE MODULATION SIGNAL:

$$e_{PM}(t) = \frac{2}{\pi} E_2 \left(\sin 2\pi 25t - \frac{1}{2} \sin 4\pi 25t + \frac{1}{3} \sin 6\pi 25t \cdots\right)$$

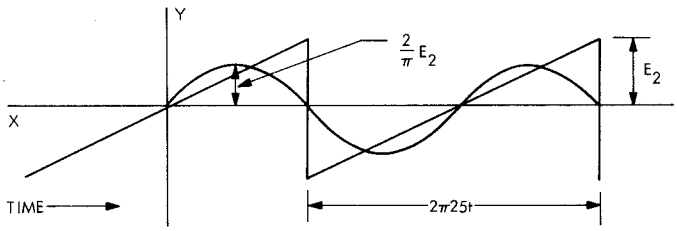


**Fig. 10. Phase modulation signal for simulating spin modulation effect**

FOURIER SERIES FOR AMPLITUDE MODULATION SIGNAL:

$$e_{AM}(t) = \frac{2}{\pi} E_3 \left(1 + \frac{2}{3} \cos 4\pi 12.5t - \frac{2}{15} \cos 8\pi 12.5t + \cdots\right)$$

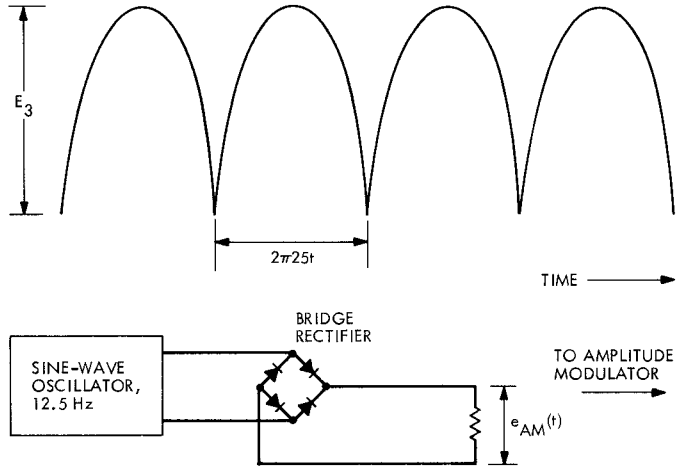


**Fig. 11. Amplitude modulation signal for simulating spin modulation effect**

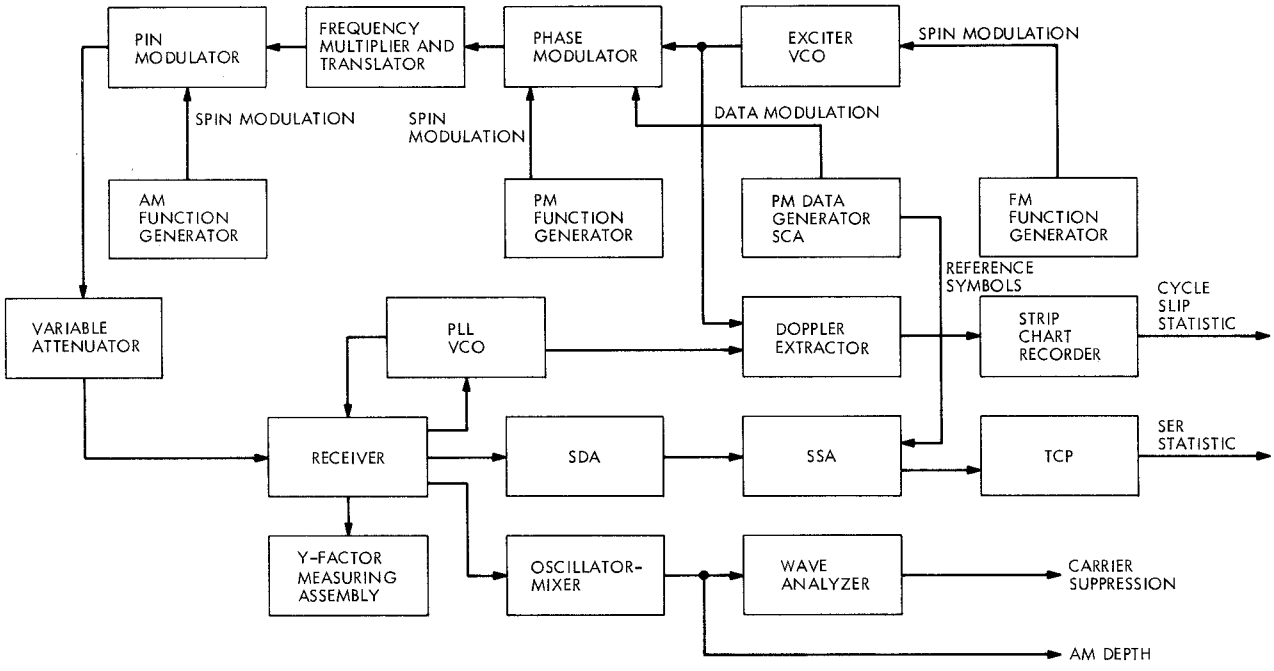


**Fig. 12. Block diagram of system test configuration**

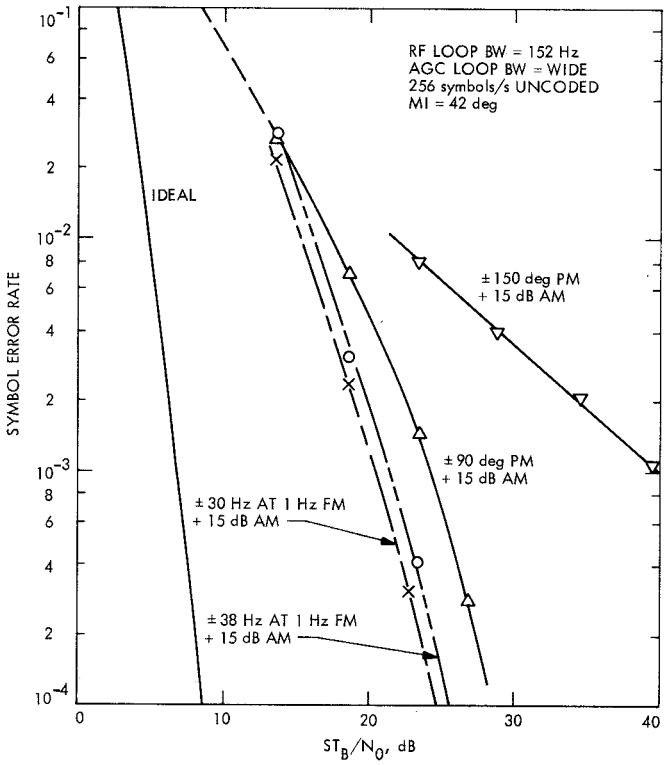


Fig. 13. Spin modulation effects under worst-case conditions

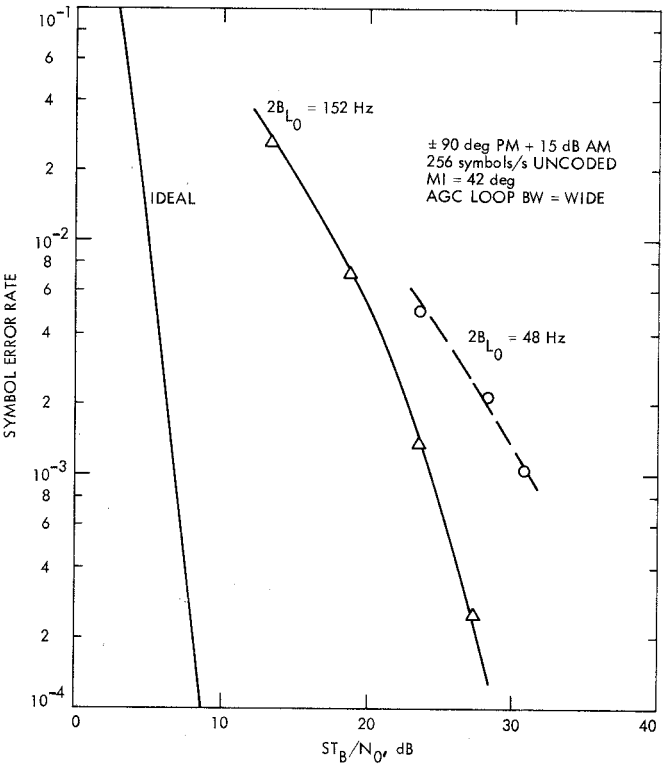


Fig. 14. BER vs SNR with spin modulation for two loop bandwidths

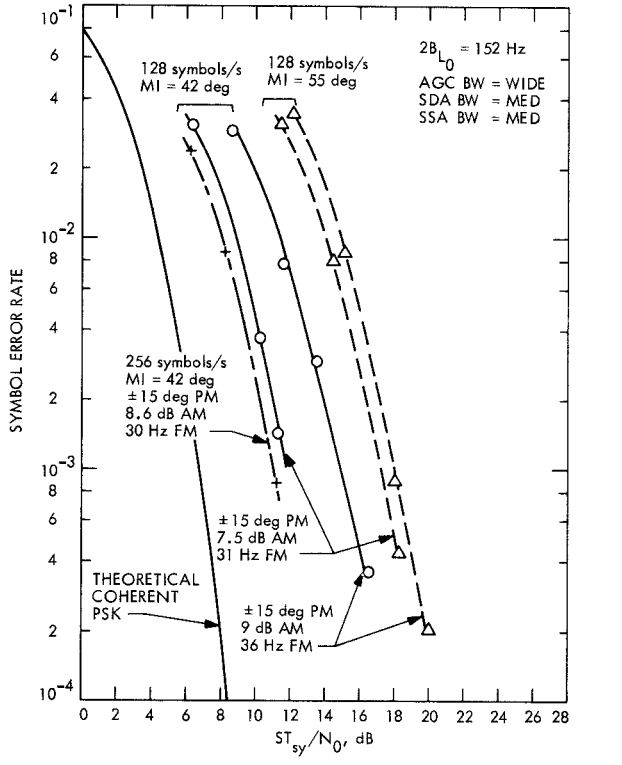


Fig. 15. Spin modulation effects for linear polarization

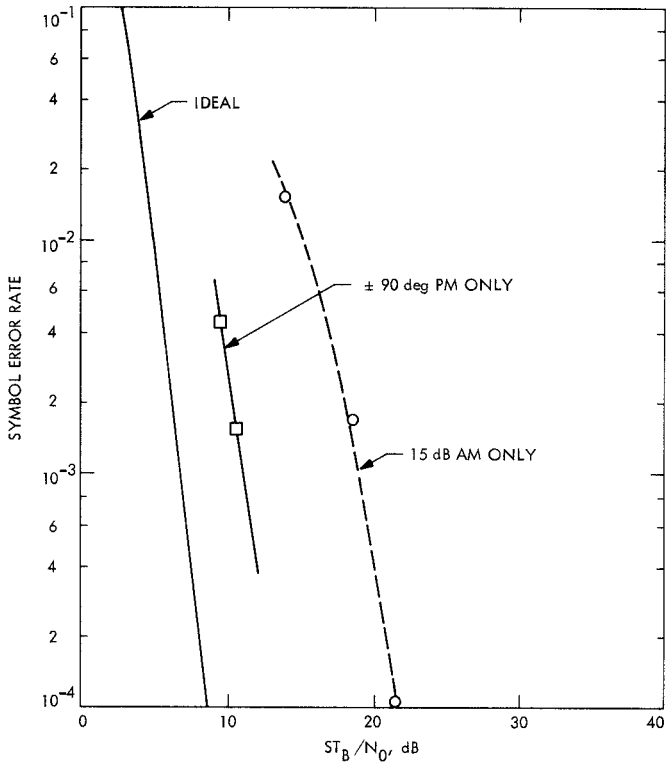


Fig. 16. BER vs $ST_B/N_0$ with AM and PM spin modulation

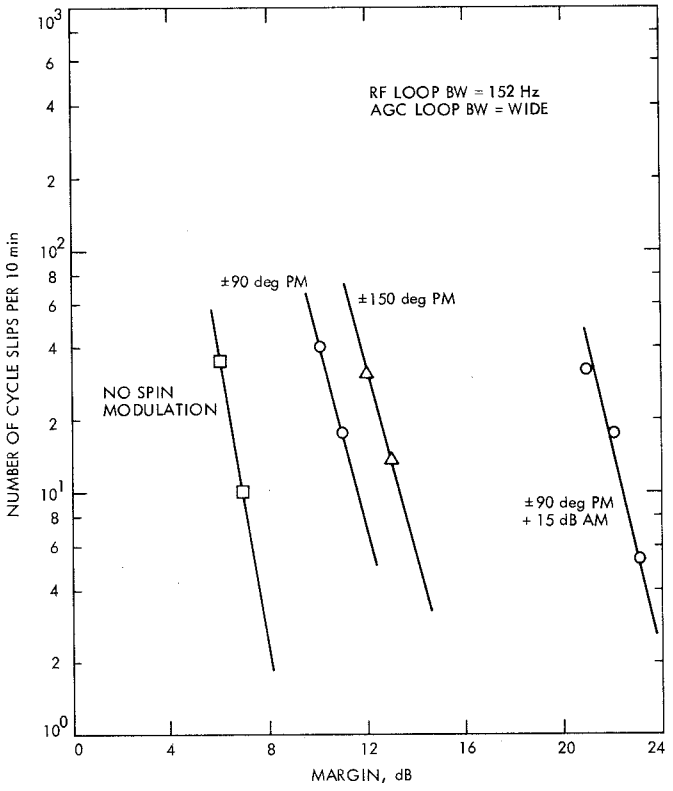


**Fig. 17. RF loop cycle slippage vs spin modulation**

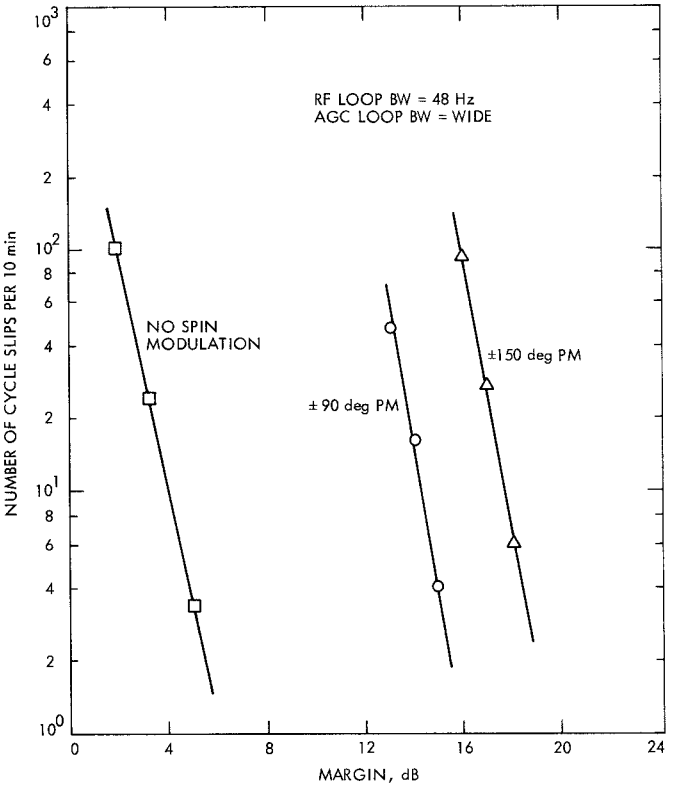


**Fig. 18. RF loop cycle slippage vs phase spin modulation**

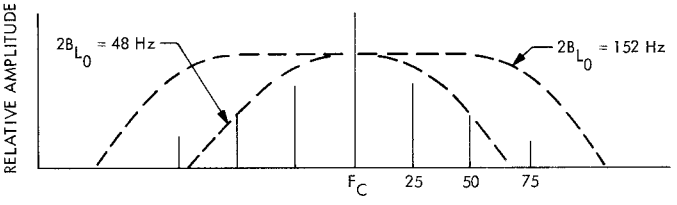


MODULATING SIGNAL: $e_{PM}(t) = \frac{2}{\pi} E_2 \left(\sin 2\pi 25t - \frac{1}{2}\sin 4\pi 25t + \frac{1}{3}\sin 6\pi 25t\right)$

$F_C$ = CARRIER FREQUENCY

**Fig. 19. Sawtooth spin modulation spectrum and receiver loop bandwidth response**